Accepted Manuscript

A novel low loss and low temperature sintering $Li_3(Mg_{1-x}Ca_x)_2NbO_6$ microwave dielectric ceramics by doping LiF additives

Ping Zhang, Kexin Sun, Lu Liu, Mi Xiao

PII: S0925-8388(18)32338-7

DOI: 10.1016/j.jallcom.2018.06.217

Reference: JALCOM 46553

To appear in: *Journal of Alloys and Compounds*

Received Date: 31 March 2018

Revised Date: 4 June 2018

Accepted Date: 18 June 2018

Please cite this article as: P. Zhang, K. Sun, L. Liu, M. Xiao, A novel low loss and low temperature sintering $Li_3(Mg_{1-x}Ca_x)_2NbO_6$ microwave dielectric ceramics by doping LiF additives, *Journal of Alloys and Compounds* (2018), doi: 10.1016/j.jallcom.2018.06.217.

A novel low loss and low temperature sintering $Li_3(Mg_{1-x}Ca_x)_2NbO_6$ microwave dielectric ceramics by doping LiF additives

Ping Zhang*, Kexin Sun, Lu Liu, Mi Xiao

School of Electrical and Information Engineering and Key Laboratory of Advanced Ceramics and Machining Technology of Ministry of Education, Tianjin University, Tianjin 300072, P. R. China

ABSTRACT

The $Li_3(Mg_{1-x}Ca_x)_2NbO_6(0.02\leq x \leq 0.08)$ ceramics were prepared through a solid-state reaction method. The effects of Ca^{2+} substitution for Mg^{2+} on the phase composition, microstructure and microwave dielectric properties of $Li_3(Mg_{1-x}Ca_x)_2NbO_6$ ceramics were investigated systematically. The XRD results showed that all the samples remained a single $Li_3Mg_2NbO_6$ phase with orthorhombic structure and Ca^{2+} ions can result in the expansion of unit cells when sintered at 1060-1220^{o}C for 6h. In this study, the change trend of the porosity-corrected permittivity showed that the permittivity of samples was mainly relative to density, not to ionic polarizability. The variation of Q×*f* values also exhibited a similar trend as that of density. The τ_f values were in accordance with the porosity-corrected permittivity. Excellent microwave dielectric properties of ε_r ~ 16.81, Q×*f* ~ 122,082 GHz, τ_f ~ -25.8 ppm/^{o}C were obtained in the x=0.04 sample when sintered at 1140^{o}C for 6h. In addition, various amounts of LiF were used as sintering additive to reduce the sintering temperature in $Li_3(Mg_{0.96}Ca_{0.04})_2NbO_6$ ceramics . The best microwave dielectric properties of ε_r ~ 15.85, Q×*f* ~ 98,012 GHz, τ_f ~ -28.6 ppm/^{o}C appeared to be $Li_3(Mg_{0.96}Ca_{0.04})_2NbO_6$ ceramics with 6wt.% LiF sintered at 900^{o}C. Besides, this composition was compatible with Ag electrode, demonstrating that it could be a promising candidate material for LTCC applications.

*Corresponding author. Tel.: +86 13702194791
Email address: zptai@163.com (P. Zhang)

Keywords: $Li_3Mg_2NbO_6$ ceramics; Microwave dielectric properties; Low loss; LTCC

1. Introduction

With the rapid revolution of microwave components used in telecommunication and radar systems, many new microwave dielectric ceramics have attracted much scientific and commercial research interest for applications[1-6]. To meet the criteria of high signal propagation speed, good reliability, and low cost in microwave devices, these microwave materials are strongly required to possess a low dielectric constant, a high Q×*f* value, and a near zero temperature coefficient of resonant frequency. In addition, the sintering temperature of microwave ceramics should be less than 961^{o}C for co-firing with Ag electrode or 1083^{o}C for co-firing with Cu electrode for LTCC applications[7-10]. Unfortunately, most of microwave dielectric ceramics usually have a high sintering temperature (>1200^{o}C), such as $ATiO_3$ (A=Ni, Mg, Co, Mn)[11] and $Li_2Mg_3BO_6$ (B=Ti, Sr, Zr)[12] system ceramics. Generally, the widely used method to decrease the sintering temperature of ceramics is adding sintering additives, which implement is at the cost of deterioration in microwave dielectric properties. Consequently, researching and developing novel ceramics with a combination of superior properties and low sintering temperature is still an urgent work in microwave materials field.

As one of new low loss microwave materials, the $Li_3Mg_2NbO_6$ ceramics with orthorhombic structure were firstly reported by Yuan et al[13]. The ceramics sintered at 1250^{o}C for 2h had microwave dielectric properties of ε_r ~ 16.8, Q×*f* ~ 79,643 GHz, τ_f ~ -27.2 ppm/^{o}C. Later, Zuo et al[14] studied that $Li_3(Mg_{0.92}Zn_{0.08})_2NbO_6$ ceramics with 0.5wt.% $0.17Li_2O$-$0.83V_2O_5$ reduced the sintering temperature to 925^{o}C and possessed good microwave dielectric properties of ε_r ~ 14, Q×*f*~ 83,395 GHz, τ_f ~ -37.2 ppm/°C. In addition, they reported that $Li_3(Mg_{0.92}Zn_{0.08})_2NbO_6$ ceramics with 30wt.% $Ba_3(VO_4)_2$ adjusted the temperature coefficient of resonant frequency to a near zero value (τ_f~ +1.5 ppm/°C) when samples sintered at 950^{o}C for 4h. Afterwards, Wu et al[15]introduced the characterization of pure

$Li_3Mg_2NbO_6$ ceramics and Zhang et al[16] studied the microstructure and microwave dielectric properties of $Li_3Mg_2NbO_6$-based system ceramics, respectively.

However, there were few reports about improving the dielectric properties of $Li_3Mg_2NbO_6$ ceramics by Mg-site substitution. Therefore, the objective of this paper is to investigate the effects of displacing Mg^{2+} by various amounts of Ca^{2+} on the phase composition, microstructure and microwave dielectric properties of $Li_3Mg_2NbO_6$ ceramics. Furthermore, appropriate amounts of LiF additives were added to $Li_3(Mg_{0.96}Ca_{0.04})_2NbO_6$ ceramics to reduce the sintering temperature. It has been successful in lowering the sintering temperature of $BaFe_{0.5}Nb_{0.5}O_3$ and $Ca[(Li_{0.33}Nb_{0.67})_{0.9}Ti_{0.1}]O_{3-\delta}$ ceramics[17,18], respectively. The effects of LiF additives on the sintering behavior, microstructure and microwave dielectric properties of $Li_3(Mg_{0.96}Ca_{0.04})_2NbO_6$ ceramics were also investigated systematically in this paper.

2. Experimental procedures

The $Li_3(Mg_{1-x}Ca_x)_2NbO_6(0.02\leq x \leq 0.08)$ (LMN1) ceramics and $Li_3(Mg_{0.96}Ca_{0.04})_2NbO_6$ + y wt.% LiF ($2\leq x \leq 8$) (LMN2) ceramics were synthesized by the conventional solid-state sintering method, as shown in Fig.1. Firstly, high purity Li_2CO_3(99%), MgO(99%), Nb_2O_5(99.9%), $CaCO_3$(99%)were used as the raw materials and weighed according to the formula of $Li_3(Mg_{1-x}Ca_x)_2NbO_6(0.02\leq x \leq 0.08)$, and then the mixed powders were ball-milled with the deionized water for 8h in a nylon container. The obtained slurries were dried and then calcined at 950^{o}C for 4h. For one thing, the obtained powders were re-milled for 8h in the deionized water. For another thing, the $Li_3(Mg_{0.96}Ca_{0.04})_2NbO_6$ calcined powders were re-milled for 8h with various amounts of LiF additives. After being dried and sieved, the granulated powders were subsequently pressed into pellets with dimensions of 10mm in diameter and 5mm in height. These pellets were preheated at 550^{o}C for 3h to expel the binder, and then the LMN1 samples were sintered at 1060-1220^{o}C for 6h while the LMN2 specimens were sintered in the

temperature range of 875°C-975°C for 6h with all the heating rate of 3°C/min. In order to reduce the lithium evaporation[19], we pressed the granulated powders into a ceramic sheet with dimensions of 10mm in diameter and 1.5mm in height. As shown in Fig.2, these pellets were placed between two ceramic sheets of the same composition during the whole sintering process.

The crystal structure of sintered samples was identified by an x-ray diffraction (XRD, Rigaku D/max 2550 PC, Tokyo, Japan). From the x-ray diffraction, the lattice parameters and unit cell volume of samples were determined by Jade6.0 software. Microstructure observation of the specimens was performed by a scanning electron microscopy (SEM, ZEISS MERLIN Compact, Germany). The permittivity and Q×*f* values at microwave frequencies were measured by a network analyzer (N5234A, Agilent Co, America) in the frequency range of 7-13GHz. The τ_f values were measured in the temperature range from 25°C to 85°C. It was calculated by the following formula:

$$\tau_f = \frac{f_2 - f_1}{f_1(T_2 - T_1)} \times 10^6 \text{ (ppm/ °C)} \quad (1)$$

where f_1 and f_2 were the corresponding resonance frequency at the temperature of T_1 and T_2, respectively.

The apparent densities were measured by Archimedes method at room temperature. The relative densities were obtained from the ratio of the apparent densities and the theoretical densities, and the theoretical densities were calculated from the crystal structure and atomic weight by Eq. (2):

$$\rho_{theo} = \frac{ZA}{V_C N_A} \quad (2)$$

where *Z*, *A*, V_C and N_A are number atoms in unit cell, atomic weight, volume of unit cell, and avagadro number, respectively.

3. Results and discussions

Fig.3 shows the XRD patterns of LMN1 ceramics sintered at 1140°C for 6h. All the reflection peaks are

well indexed based on the JCPDS file number 86-0346 for $Li_3Mg_2NbO_6$ phase with orthorhombic structure, which belongs to the space group Fddd (70). And there are no obvious additional phases being detected throughout the substitution range from 0.02 to 0.08. In particular, the strongest diffraction peak gradually shifts toward a lower angle direction as x value increases. According to the Bragg equation, the interplanar spacing becomes larger, indicating that the unit cell volume increases slightly with the increasing x values, which is in accordance with the results as shown in Table 1. The cell volume progressively increases from 894.45$Å^3$ at x=0.02 to 898.13$Å^3$ at x=0.08, which could be due to that the radius of Ca^{2+} (1.00Å) is larger than that of Mg^{2+} (0.72Å). All these results indicate that the $Li_3(Mg_{1-x}Ca_x)_2NbO_6$ ceramic solid solutions are formed during the whole substitution range.

The SEM images of LMN1 samples sintered at 1140^oC are shown in Fig.4(a)-(d). All the samples exhibit a closely packed grain morphology and discernable grain boundaries. The sample with x=0.02 sintered at 1140 ^oC shows a relatively densified microstructure but with uneven particle size (5-30μm) as shown in Fig.4(a). With the increase of Ca^{2+} content, the small grains grow rapidly and well homogeneous morphology with the particle size(20-35μm) can be obtained in the x=0.04 sample as shown in Fig.4(b). However, further raising the Ca^{2+} content results in that the particle size becomes more uneven, as shown in Fig.4(c) and (d). And similar phenomenon appears in the $Mg_{1-x}Ca_xZrTa_2O_8$ ceramics[20]. Thus, Ca^{2+} substitution for Mg^{2+} with x=0.04 has an important role in promoting the grain growth, whereas excessive Ca^{2+} ions deteriorate the homogeneous distribution of ceramic grains. Furthermore, to clarify the morphological changes in LMN1 ceramics with sintering temperature, the surface micrographs of the x=0.04 sample sintered at various temperatures are illustrated in Fig.4(b), (e) and (f). For the sample sintered at 1060^oC, small grains with highly porous morphology could be clearly noticed in Fig.4(e). As the temperature increases, the grains grow rapidly and all pores

disappear on the surface of samples at 1140°C in Fig.4(b). However, when the sintering temperature increases to 1220°C, abnormal grain growth appears in the specimen. Some grains are melted and ambiguous grain boundaries are observed in Fig.4(f). It might be an indication of over sintering. Therefore, the densified microstructure with uniform and big grains could be achieved at 1140°C and with x=0.04, as shown in Fig.4(b).

In order to characterize the effects of Ca^{2+} substitution on the particle size of LMN1 ceramics, the approximate statistical distribution of particle size of samples sintered at 1140 °C with different x values measured by Nano Measurer software is displayed in Fig.5(a). The particle size of all grains was measured according to SEM images. As shown in Fig.5(a), when all samples sintered at 1140 °C, the particle size is more uniform with x=0.02 and x=0.04. However, the particle size becomes uneven with x=0.06 and x=0.08. Herein, the dispersion degree of distribution of particle size (σ) is used to check the uniformity of particle size. The formula in the reference is

$$\overline{S} = \frac{1}{n}\sum_{i=1}^{n} S_i \tag{3}$$

$$\sigma = \sqrt{\frac{\sum_{i=1}^{n}(S_i - \overline{S})^2}{n}} \tag{4}$$

where $\overline{S}$ and σ are average particle size and dispersion degree of distribution of particle size respectively. As plotted in Fig.5(b), the average particle size increases at first with x from 0.02 to 0.06 and then drops precipitously when x=0.08. The values are about18.81μm with x=0.02, 25.41μm with x=0.04, 27.21μm with x=0.06, 19.04μm with x=0.08, respectively. The dispersion degree (σ) is the smallest with x=0.04 and is the largest with x=0.06, which illustrates that the distribution of particle size gradually becomes inhomogeneous as a function of x value. In

summary, the particle size is larger and uniform when x=0.04.

Fig.6 shows the relative density and permittivity of LMN1 ceramics with different x values sintered at various sintering temperatures for 6h. The relative densities of all samples increase rapidly as the sintering temperature increase from 1060^{o}C to 1100^{o}C and reach the maximum value at 1140^{o}C. Further raising the temperature would reduce the density slightly. The relative density curve of LMN1 ceramics matches well with the SEM pictures where the uneven particle size and pores lead to the low density. The permittivity presents a similar variation trend with that of relative density, which initially increases with increasing temperature and then gradually decreases after reaching the maximum value. In general, the permittivity is mainly dependent on the density, secondary phase, and ionic polarizability of the ceramics[21, 22]. In this paper, the permittivity of LMN1 ceramics is significantly determined by the density of samples. The maximum permittivity of 16.81 appears in the composition of $Li_3(Mg_{0.96}Ca_{0.04})_2NbO_6$ ceramic sintered at 1140^{o}C for 6h.

The ionic polarizability of Ca^{2+} is larger than that of Mg^{2+}. However, the permittivity of ceramic samples with the same sintering temperature did not increase with the increase of Ca^{2+} content, which mainly results from that the ceramic samples with x = 0.06 and x = 0.08 have a relatively low density (less than 3.65g /cm^3). In order to verify the effect of density on the permittivity, we modified the theoretical permittivities of LMN1 ceramics sintered at 1140^{o}C for 6h by the Bruggeman method. The results are shown in Table 2. The theoretical ionic polarizabilities (α_{theo}) of ceramics were calculated from the Shannon's additivity rule of the ionic polarizabilities of corresponding ions, according to the following formula:

$$\alpha_{theo} = 3\alpha Li^{+}+2(1-x)\alpha Mg^{2+}+2x\alpha Ca^{2+}+\alpha Nb^{5+}+6\alpha O^{2-} \quad (5)$$

The theoretical permittivities (ε_{theo}) of ceramics were calculated by using the theoretical ionic

polarizabilities (α_{theo}) and the unit of molar volume of ceramics according to the Clausius-Mosotti equation:

$$\varepsilon_{theo} = \frac{3V_m + 8\pi\alpha_{theo}}{3V_m - 4\pi\alpha_{theo}} \quad (6)$$

As shown in Table 2, it is easy to find the theoretical permittivities of ceramics gradually increase with the increasing x values. Considering the effect of porosity, the theoretical permittivities were corrected by the Bruggeman effective medium approximation[23]:

$$(1-f)\frac{\varepsilon_{theo} - \varepsilon_{pc}}{\varepsilon_{theo} + 2\varepsilon_{pc}} + f\frac{\varepsilon_{air} - \varepsilon_{pc}}{\varepsilon_{air} + 2\varepsilon_{pc}} = 0 \quad (7)$$

where ε_{pc} are the porosity-corrected permittivity of ceramics. ε_{air} and f are the relative permittivity and volume fraction of air in the microwave dielectric ceramics, respectively. The pore-corrected permittivity of ceramics sintered at 1140^{o}C for 6h is achieved and plotted in Fig.7. Simultaneously, the measured permittivity is also given in Fig.7. As depicted in Fig.7, with the increase of Ca^{2+} content, the pore-corrected permittivity of LMN1 ceramic shows the approximately same trend as the measured permittivity, which is slightly smaller than the measured ε_r value. Although Ca^{2+} with higher ionic polarizability (3.17Å^3) replaces Mg^{2+} (1.33Å^3) with lower ionic polarizability, the density of the ceramics is smaller and smaller when x=0.06 and x=0.08, so the pore-corrected permittivity becomes smaller, implying that the density is a dominating factor to control the permittivity in LMN1 ceramics.

Fig.8 reveals the Q×f values of LMN1 ceramics sintered at various sintering temperatures for 6h. For all compositions, The Q×f values firstly increase with the increase of sintering temperature, reaching a maximum value when the sintering temperature is at 1140^{o}C. And then the Q×f values gradually decrease as the sintering temperature further increases. Usually, the Q×f value is strongly influenced by

intrinsic factors such as ionic polarization and crystalline structure, as well as an extrinsic loss which includes secondary phases, grain size, distribution of grain size, grain boundary, oxygen vacancy and porosity[24]. The Q×*f* values of all samples exhibit a similar tendency as the variation in density. Except for the effect of secondary phases in pure LMN1 ceramics, taking Fig.5 into account, the main factors determining the Q×*f* value of LMN1 ceramics are detected to be the density, particle size and distribution of particle size. The maximum Q×*f* value of 122,082GHz is achieved in the x=0.04 sample sintered at 1140^{o}C for 6h. The first increment of Q×*f* value would be correlated with an increase in densification and particle size, which reduce the imperfections caused by porosity and grain boundaries in the crystal structure [25-28], while the reduction of Q×*f* value would be related to the low density and disharmonious microstructure, as shown in Fig.4(d), resulting in a high loss of material. These above results imply that small amount of Ca^{2+} could effectively promote the Q×*f* values, whereas excessive Ca^{2+} substitution for Mg^{2+} would deteriorate the microwave dielectric properties of LMN1ceramics.

Generally, the τ_f value of microwave dielectric ceramics is mainly determined by its temperature coefficient of dielectric constant τ_ε and thermal expansion coefficient α_L, as shown in the following equation:

$$\tau_f = -(\frac{\tau_\varepsilon}{2} + \alpha_L) \tag{8}$$

While, Harrop reported the relationship between ε_{pc} and τ_ε can be described as follow[29]:

$$\tau_\varepsilon = -\alpha_L \varepsilon_{pc} \tag{9}$$

where ε_{pc} is the pore-corrected permittivity calculated in Table 2. These above two equations show that τ_f and ε_{pc} of microwave dielectric ceramics are positively related. Fig.9 shows the τ_f and ε_{pc} values of LMN1ceramics sintered at 1140^{o}C for 6h, which is in accordance with the above derivation. The τ_f values of LMN1ceramics vary in the range from -23.2 ppm/^{o}C to -27.4 ppm/^{o}C as x from 0.02 to 0.08.

In addition, there is a report in the literature including that similar conditions have appeared in $Mg_{1-x}Ca_xZrTa_2O_8$ ceramics, which shows that the ε_{pc} value is an important factor affecting its τ_f value in the $Li_3(Mg_{1-x}Ca_x)_2NbO_6$ ceramic system. In summary, optimum microwave dielectric properties of ε_r ~ 16.81, $Q \times f$ ~ 122,082 GHz, τ_f ~ -25.8 ppm/^{o}C are obtained in $Li_3(Mg_{0.96}Ca_{0.04})_2NbO_6$ ceramics when sintered at 1140^{o}C for 6h.

In order to meet the requirement for LTCC applications, the sintering temperature of ceramics should be lowered below 961^{o}C for co-firing with Ag electrode. Generally, the most frequently used method is adding low-melting glasses or metal oxides to reduce the sintering temperature. In the present study, various amounts of LiF additives are used as sintering aid to reduce the sintering temperature of $Li_3(Mg_{0.96}Ca_{0.04})_2NbO_6$ ceramics.

Fig.10 shows the XRD patterns of LMN2 ceramics sintered at 900^{o}C for 6h. All the XRD patterns show a single $Li_3Mg_2NbO_6$ phase and no obvious LiF phase is detected, which demonstrates that LiF additives have no chemical reactions with LMN2 ceramics and only exist as a liquid phase during the whole sintering process.

Fig.11 illustrates the SEM images of LMN2 ceramics sintered at 900^{o}C for 6h. As shown in Fig.11(a), the grains are small and many pores could be seen clearly in the sample. With the increase of LiF content, the grains grow rapidly, the pores disappear and compacted microstructures are achieved in the ceramics, as confirmed in Fig.9(b)-(d). Especially the sample doped with 6wt.% LiF has a more uniform microstructure with the particle size of 10-15μm at 900^{o}C. Further increasing the amount of LiF additives would inhibit the grain growth, leading to a decrease in particle size, as shown Fig.9(d). Based on these results, It can be found that the preparation of $Li_3(Mg_{0.96}Ca_{0.04})_2NbO_6$ ceramics with high densification could be realized by adding the appropriate amount of LiF additives.

Fig.12 shows the relative densities and microwave dielectric properties of LMN2ceramics sintered at various sintering temperatures for 6h. As shown in Fig.12(a), the relative densities of samples with 2wt.% LiF additives become larger as the sintering temperature increases, but still relatively small overall, which indicates that 2wt.% LiF is not enough to densify the ceramics efficiently at the low sintering temperature. Continuing to raise the content of LiF, the relative density rises rapidly and the optimum sintering temperature could be effectively reduced to 900^{o}C when 6wt.% LiF additives are used. However, the densification decreases slightly as the amount of LiF additives reaches 8wt.%. It might be due to the comparatively lower theoretical density of LiF additives(2.64g/cm^3)[30], which has an obvious influence on degrading the density when massive LiF is added into the ceramics. The maximum density of 3.554g/cm^3 is achieved for 6wt.% LiF modified sample when sintered at 900^{o}C for 6h. These results confirm that low temperature sintering of $Li_3(Mg_{0.96}Ca_{0.04})_2NbO_6$ ceramics could be realized by doping appropriate amount of LiF additives. Variations of permittivity with sintering temperature are shown in Fig.12(b). The relationship between ε_r values and LiF content reveals almost the same trend as that between density and LiF content. This similar tendency confirms that density plays a critical role in controlling the permittivity of LMN2 ceramics. Comparatively, the permittivity firstly increases with the increasing amount of LiF additives, and then decreases slightly with subsequent increase of LiF content. The maximum value of 15.85 is obtained in 6wt.% LiF added sample. The Q×*f* values of the LMN2 compositions sintered at 875-975^{o}C are shown in Fig.12(c). In this study, the Q×*f* values are mainly dependent on extrinsic factors. The beginning increase of Q×*f* values with raising LiF content could be ascribed to the promotion in particle size as shown in Fig.11(b) and (c), while the subsequent decline in Q×*f* values might be correlated with the low density, as shown in Fig.12(a). The maximum value of 98,012 GHz is obtained for the sample with 6wt.% LiF additives

sintered at 900°C.

Fig.13 shows the τ_f values of LMN2ceramics sintered at 900°C for 6h. The τ_f values present a descending tendency with increasing LiF content, which implys that abundant LiF additives are harmful to the stability of resonant frequency for LMN2 ceramics. In summary, the $Li_3(Mg_{0.96}Ca_{0.04})_2NbO_6$ ceramics doped with 6wt.% LiF additives sintered at 900°C for 6h reveal excellent microwave dielectric properties of ε_r ~ 15.85, Q×f ~98,012 GHz, τ_f ~ -28.6 ppm/°C.

To test the chemical compatibility between ceramics and Ag powders, the 6wt.% LiF additives modified $Li_3(Mg_{0.96}Ca_{0.04})_2NbO_6$ ceramic sheet and Ag powders are co-fired at 900°C for 6h. The corresponding XRD pattern(Fig.14) presents that the co-fired ceramics consist of the $Li_3Mg_2NbO_6$ and Ag phase, Furthermore, the obtained EDS image(Fig.15) reveals that the boundary between ceramic and silver is clear, and the intensity of the line scanning diffraction peak of Ag changes sharply at the cross section, which indicates that silver does not diffuse into the ceramic during the sintering process, and also indicates that LMN2 ceramics have good chemical compatibility with silver electrodes, which would be a promising potential material for LTCC applications.

4. Conclusions

The $Li_3(Mg_{1-x}Ca_x)_2NbO_6$ ceramics are prepared by the conventional solid state reaction method. The effects of Ca^{2+} substitution on the phase structure, microstructure and microwave dielectric properties are investigated systematically. The XRD patterns show that all the compounds perform a single $Li_3Mg_2NbO_6$ phase with orthorhombic structure. Excellent microwave dielectric properties of ε_r ~ 16.81, Q×f ~ 122,082 GHz, τ_f ~ -25.8 ppm/°C are realized in the $Li_3(Mg_{0.96}Ca_{0.04})_2NbO_6$ sample when sintered at 1140°C for 6h. In addition, various amounts of LiF additives are used to reduce the sintering temperature of $Li_3(Mg_{0.96}Ca_{0.04})_2NbO_6$ ceramics for practical applications. Particularly, the 6wt.% LiF

additives doped $Li_3(Mg_{0.96}Ca_{0.04})_2NbO_6$ ceramics sintered at 900^oC for 6h exhibit superior microwave dielectric properties of ε_r ~ 15.85, Q×f ~ 98,012 GHz, τ_f ~ -28.6 ppm/^oC, which might be selected as a promising candidate material for LTCC applications.

Acknowledgments

This work was supported by the National Natural Science Foundation of China（No. 61671323）

References

[1] P. Zhang, Y.G. Zhao, J. Liu, Z. Song, X. Wang, Enhanced microwave dielectric properties of $NdNbO_4$ ceramic by Ta^{5+} substitution, J. Alloys Compd. 640 (2015) 90-94.

[2] P. Zhang, Y.G. Zhao, X.Y. Wang, The correlations between electronic polarizability, packing fraction, bond energy and microwave dielectric properties of $Nd(Nb_{1-x}Sb_x)O_4$ ceramics, J. Alloys Compd. 644 (2015) 621-625.

[3] P. Zhang, Y.G. Zhao, Effects of structural characteristics on microwave dielectric properties of $Li_2Mg(Ti_{1-x}Mn_x)_3O_8$ ceramics, J. Alloys Compd. 647 (2015) 386-391.

[4] P. Zhang, Y.G. Zhao, H.T. Wu, X.Y. Wang, New temperature stable and low loss materials of $(Nd_{0.97}Mn_{0.045})_{1.02}Nb_{0.988}O_4$ ceramics by La^{3+} substitution, J. Alloys Compd. 650 (2015) 547-552.

[5] I. M. Reaney, D. Iddles, Microwave dielectric ceramics for resonators and filters in mobile phone networks, J. Am. Ceram. Soc. 89 (2006) 2063-2072.

[6] X. Chen, W. Zhang, B. Zalinska, Low sintering temperature microwave dielectric ceramics and composites based on Bi_2O_3-B_2O_3, J. Am. Ceram. Soc. 95 (2012) 3207-3213.

[7] X. Chen, W. Zhang, S. Bai, Densification and characterization of SiO_2-B_2O_3-CaO-MgO glass/Al_2O_3 composites for LTCC application, Ceram. Int. 39 (2013) 6355-6361.

[8] L.X. Pang, W.G. Liu, D. Zhou, Z.X. Yue, Novel glass-free low-temperature fired microwave dielectric ceramics: Bi $(Ga_{1/3}Mo_{2/3})$ O_4, Ceram. Int. 42 (2016) 4574-4577.

[9] C.X. Su, L. Fang, Z.H. Wei, X.J. Kuang, $LiCa_3ZnV_3O_{12}$: a novel low-firing, high Q microwave dielectric ceramic, Ceram. Int. 40 (2014) 5015-5018.

[10] M.T. Sebastian, Elsevier Science Technology Publications, Oxford, 2008.

[11] E.S. Kim, C.J. Jeon, Microwave dielectric properties of $ATiO_3$ (A= Ni, Mg, Co, Mn) ceramics, J. Eur. Ceram. Soc. 30 (2010) 341-346.

[12] H.T. Wu, E.S. Kim, Correlations between crystal structure and dielectric properties of high-Q materials in rock-salt structure $Li_2O–MgO–BO_2$ (B= Ti, Sn, Zr) systems at microwave frequency, RSC. Adv. 6 (2016) 47443-47453.

[13] L.L. Yuan, J.J. Bian, Microwave dielectric properties of the lithium containing compounds with rock salt structure, Ferroelectrics. 387 (2009) 123-129.

[14] T.W. Zhang, R.Z. Zuo, C. Zhang, Preparation and microwave dielectric properties of $Li_3(Mg_{0.92}Zn_{0.08})_2NbO_6–Ba_3(VO_4)_2$ composite ceramics for LTCC applications, Mater. Res. Bull. 68 (2015) 109-114.

[15] H.T. Wu, E.S. Kim, Characterization of low loss microwave dielectric materials $Li_3Mg_2NbO_6$ based on the chemical bond theory, J. Alloys Compd. 669 (2016) 134-140.

[16] Y.G. Zhao, P. Zhang, Microstructure and microwave dielectric properties of low loss materials $Li_3(Mg_{0.95}A_{0.05})_2NbO_6$ (A= Ca^{2+}, Ni^{2+}, Zn^{2+}, Mn^{2+}) with rock-salt structure, J. Alloys Compd. 658 (2016) 744-748.

[17] U. Intatha, S. Eitssayeam, K. Pengpat, K.J.D. MacKenzie, Dielectric properties of low temperature sintered LiF doped $BaFe_{0.5}Nb_{0.5}O_3$, Mater. Lett. 61 (2007) 196-200.

[18] J.X. Tong, Q.L. Zhang, H. Yang, J.L. Zou, Low-temperature firing and microwave dielectric properties of $Ca[(Li_{0.33}Nb_{0.67})_{0.9}Ti_{0.1}]O_{3-\delta}$ ceramics with LiF addition, Mater. Lett. 59 (2005)3252-3255.

[19] J. Zhang, R.Z. Zuo, Synthesis and microwave dielectric properties of $Li_2Mg_2(WO_4)_3$ ceramics,

Mater. Lett. 158 (2015) 92-94.

[20] Y.J. Lin, S.F. Wang, B.C. Lai, Y.X. Liu, Densification, microstructure evolution, and microwave dielectric properties of $Mg_{1-x}Ca_xZrTa_2O_8$ ceramics, Eur. Ceram. Soc. 37 (2017) 2825-2831.

[21] R.D. Shannon, G.R. Rossman, Dielectric constants of silicate garnets and the oxide additivity rule, Am. Mineral. 77 (1992) 94-100.

[22] E.S. Kim, S.H. Kim, K.H. Yoon, Dependence of thermal stability on octahedral distortion of $(1-x)(Ca_{0.3}Li_{0.119}Sm_{0.427})TiO_3$-$xLnAlO_3$(Ln=Nd, Sm) ceramics, Ceram. Soc. Jpn. 112 (2004) S1645-S1649.

[23] D. Stroud, Stroud D, The effective medium approximations: Some recent developments, Superlattice. Microst. 23 (1998) 567-573.

[24] S.D. Ramarao, S.R. Kiran, V.R.K. Murthy, Structural, lattice vibrational, optical and microwave dielectric studies on $Ca_{1-x}Sr_xMoO_4$ ceramics with scheelite structure, J. Mater. Res. Bull. 56 (2014) 71-79.

[25] C.L. Huang, S.S. Liu, Low‐Loss Microwave Dielectrics in the $(Mg_{1-x}Zn_x)_2TiO_4$ Ceramics, Am. Ceram. Soc. 91 (2008) 3428-3430.

[26] C.L. Huang, J.Y. Chen, High-Q Microwave Dielectrics in the $(Mg_{1-x}Co_x)_2TiO_4$ Ceramics, J. Am. Ceram. Soc. 92 (2009) 379-383.

[27] C.L. Huang, J.Y. Chen, Low-Loss Microwave Dielectric Ceramics Using $(Mg_{1-x}Mn_x)_2TiO_4$ (x=0.02-0.1) Solid Solution, J. Am. Ceram. Soc. 92 (2009) 675-678.

[28] C.L. Huang, W.R. Yang, P.C. Yu, High-Q microwave dielectrics in low-temperature sintered $(Zn_{1-x}Ni_x)_3Nb_2O_8$ ceramics, J. Eur. Ceram. Soc. 34 (2014) 277-284.

[29] P.J. Harrop, Temperature coefficients of capacitance of solids, J. Mater. Sci. 4 (1969) 370-374.

[30] J. Ma, T. Yang, Z.F. Fu, P. Liu, Low-fired Mg_2SiO_4-based dielectric ceramics with temperature stable for LTCC applications, J. Alloys Compd. 695 (2017) 3198-3201.

Table1 Lattice parameters of $Li_3(Mg_{1-x}Ca_x)_2NbO_6$ ceramics sintered at 1140°C

x value	ST(°C)	a (Å)	b (Å)	c (Å)	V_{unit} (Å^3)
0.02	1140	8.549(3)	5.896(5)	17.743(1)	894.45
0.04	1140	8.548(2)	5.914(3)	17.730(6)	896.41
0.06	1140	8.546(2)	5.926(9)	17.721(4)	897.64
0.08	1140	8.542(9)	5.934(5)	17.715(1)	898.13

Table2 The pore-corrected permittivity of $Li_3(Mg_{1-x}Ca_x)_2NbO_6$ ceramics sintered at 1140°C

x value	α_{theo}	ε_{theo}	f	ε_{pc}
0.02	22.354	16.411(8)	0.043(1)	15.416(2)
0.04	22.428	16.518(1)	0.041(1)	15.585(1)
0.06	22.502	16.704(3)	0.055(1)	15.433(3)
0.08	22.576	16.976(6)	0.064(1)	15.454(0)

Figures captions

Fig.1 The synthesized processes of LMN1 and LMN2 ceramics.

Fig.2 Ceramic stacking method.

Fig.3 The XRD patterns of LMN1 ceramics sintered at 1140^{o}C for 6h.

Fig.4 The SEM images of LMN1 samples sintered at various sintering temperatures for 6h: (a)x=0.02, 1140^{o}C; (b)x=0.04, 1140^{o}C; (c)x=0.06, 1140^{o}C; (d)x=0.08, 1140^{o}C; (e)x=0.04, 1060^{o}C; (f)x=0.04, 1220^{o}C.

Fig.5 (a) particle size, (b) the average particle size and dispersion degree of particle size sintering at 1140^{o}C for 6h.

Fig.6 The bulk density and permittivity of LMN1ceramics sintered at various sintering temperatures for 6h.

Fig.7 The pore-corrected permittivity and measured permittivity of LMN1 ceramics sintered at 1140^{o}C for 6h

Fig.8 The Q×f values of LMN1 ceramics sintered at various sintering temperatures for 6h.

Fig.9 The τ_f values and pore-corrected permittivity of LMN1ceramics sintered at 1140^{o}C for 6h.

Fig.10 The XRD patterns of LMN2 ceramics sintered at 900^{o}C for 6h.

Fig.11 The SEM images of LMN2ceramics sintered at 900^{o}C for 6h: (a)2wt.%; (b)4wt.%; (c)6wt.%; (d)8wt.%.

Fig.12 The bulk density and microwave dielectric properties of LMN2ceramics sintered at various sintering temperatures for 6h.

Fig.13 The τ_f values of LMN2ceramics sintered at 900^{o}C for 6h.

Fig.14 The XRD patterns of 6wt.% LiF doped $Li_3(Mg_{0.96}Ca_{0.04})_2NbO_6$ ceramic sheet with Ag co-fired at 900^{o}C for 6h.

Fig.15 The section EDS images of 6wt.% LiF doped $Li_3(Mg_{0.96}Ca_{0.04})_2NbO_6$ ceramic sheet with Ag co-fired at 900^{o}C for 6h.

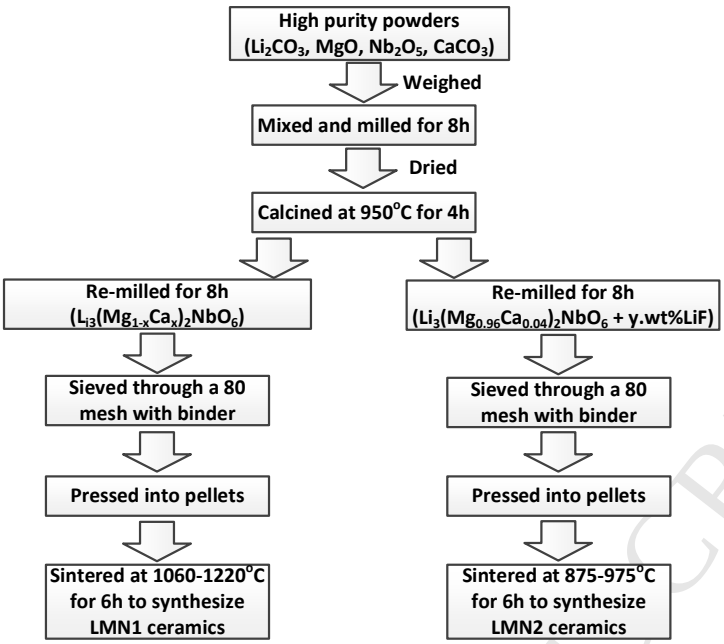

Fig.1

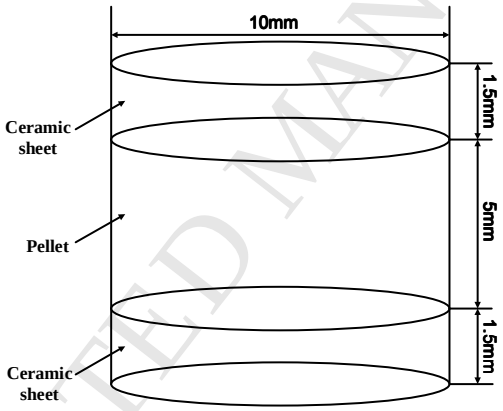

Fig.2

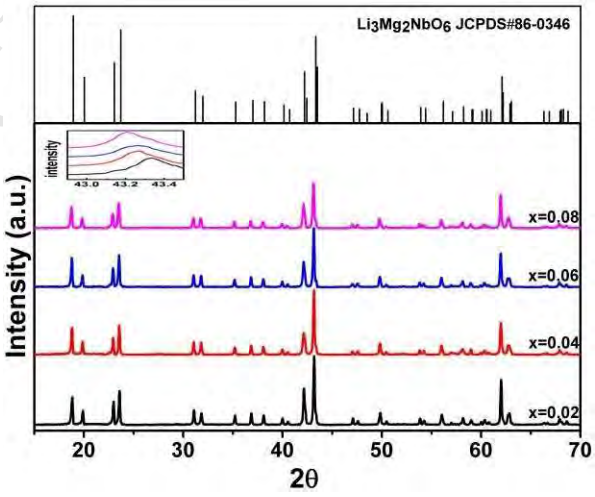

Fig. 3

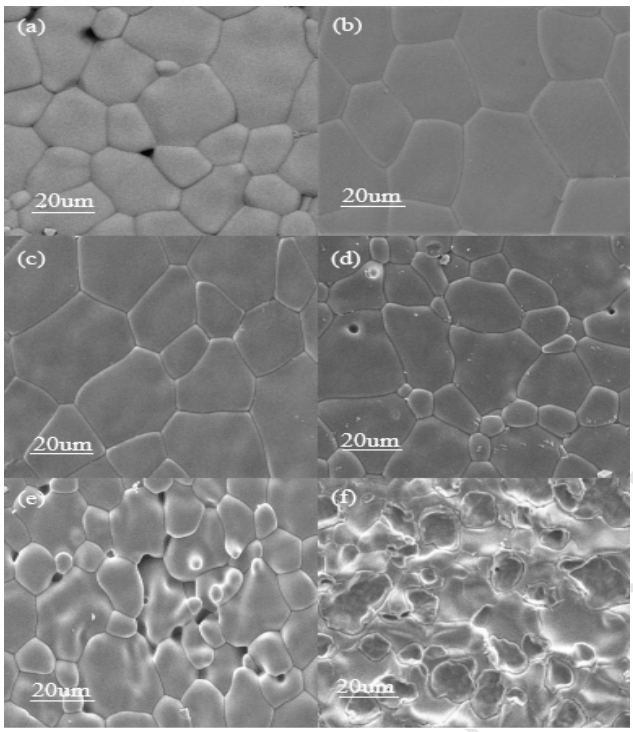
(a)
20um
(b)
20um
(c)
20um
(d)
20um
(e)
20um
(f)
20um

Fig. 4

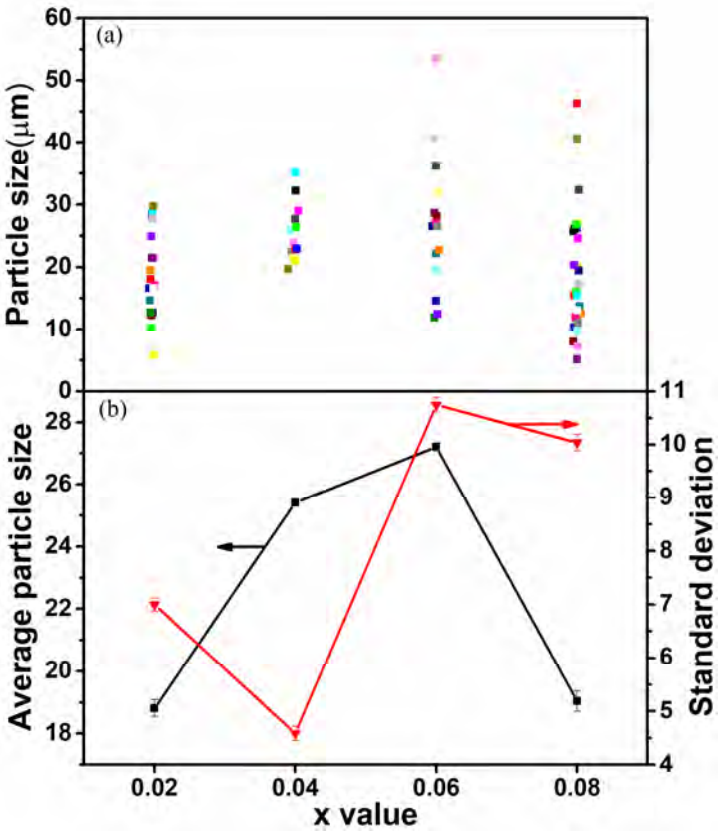
(a)
Particle size(μm)
60
50
40
30
20
10
0
(b)
Average particle size
28
26
24
22
20
18
Standard deviation
11
10
9
8
7
6
5
4
0.02
0.04
0.06
0.08
x value

Fig. 5

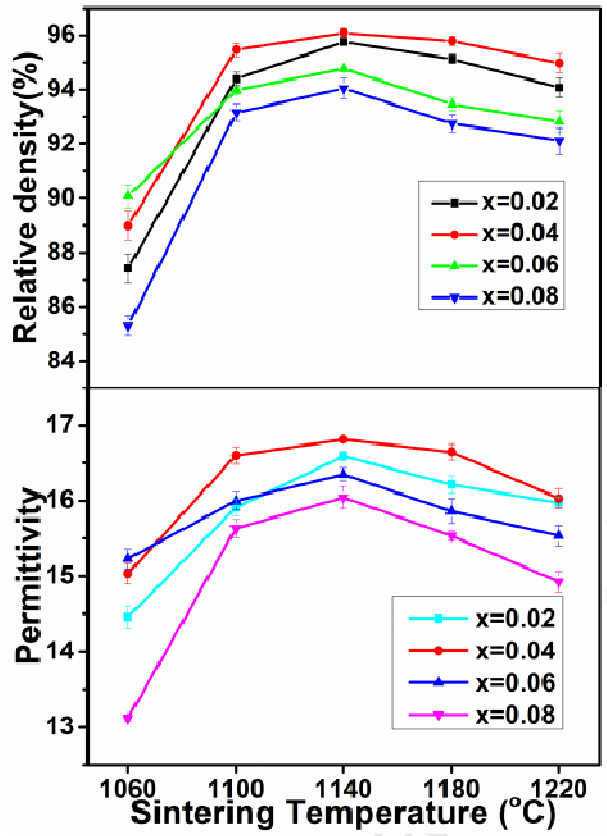
Relative density(%)
96
94
92
90
88
86
84
x=0.02
x=0.04
x=0.06
x=0.08
Permittivity
17
16
15
14
13
x=0.02
x=0.04
x=0.06
x=0.08
1060
1100
1140
1180
1220
Sintering Temperature (°C)

Fig. 6

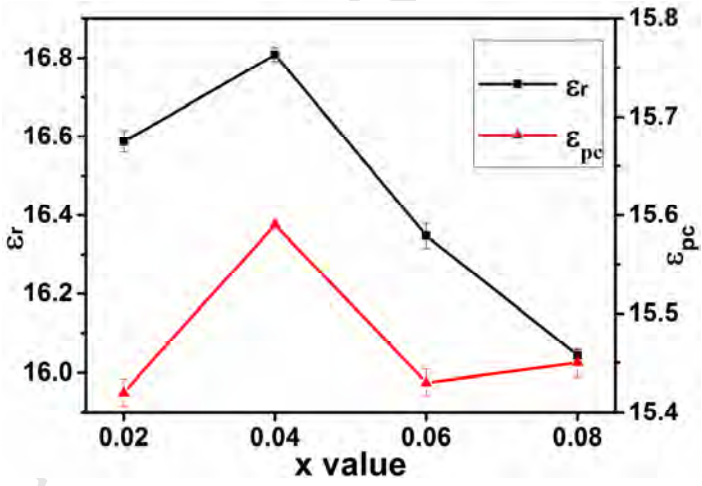
16.8
16.6
16.4
16.2
16.0
εr
15.8
15.7
15.6
15.5
15.4
εpc
εr
εpc
0.02
0.04
0.06
0.08
x value

Fig.7

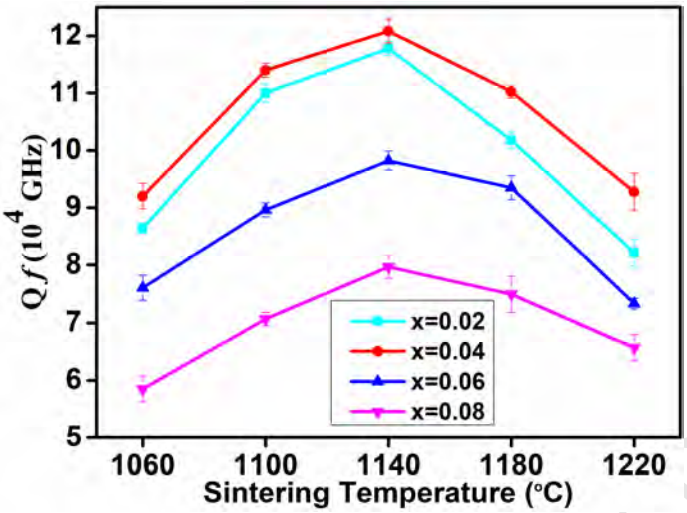

Fig. 8

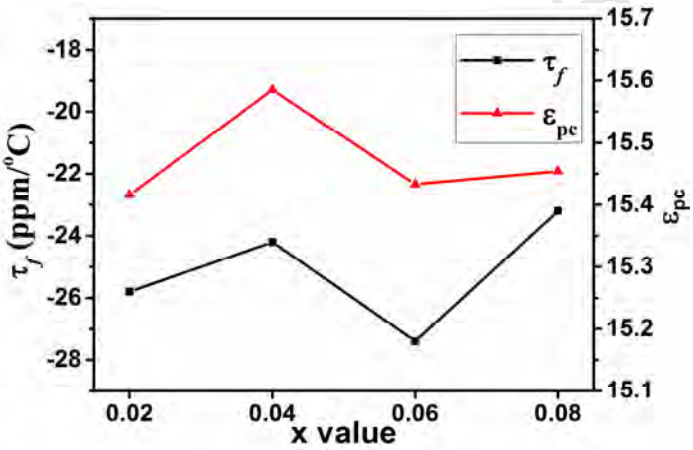

Fig. 9

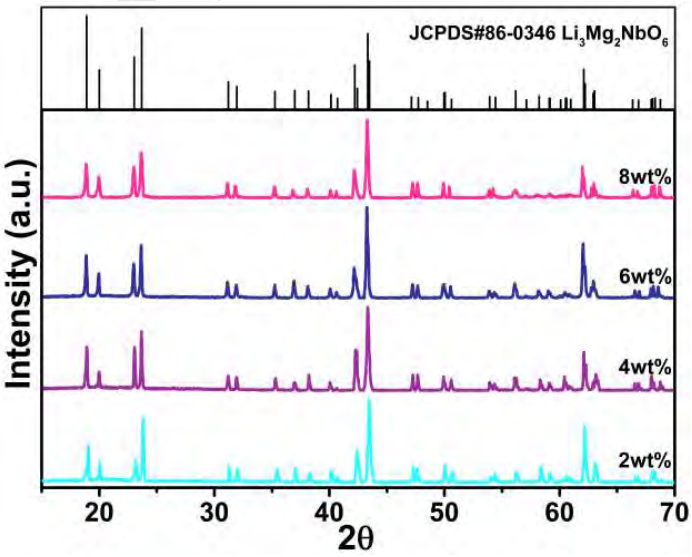

Fig. 10

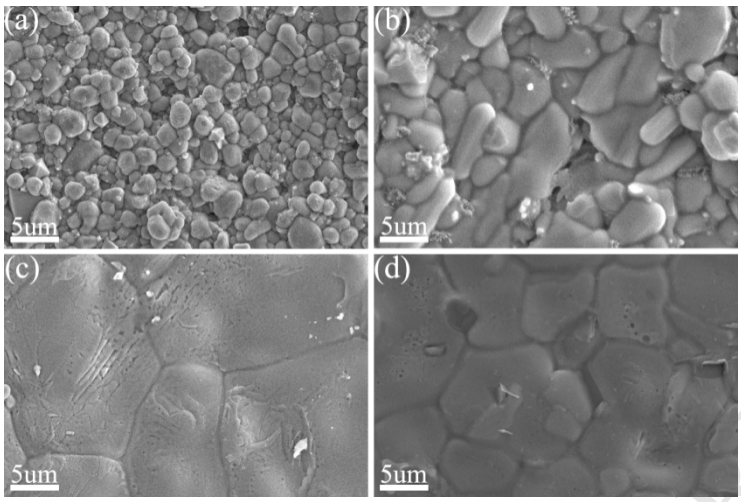
(a)
5um
(b)
5um
(c)
5um
(d)
5um

Fig. 11

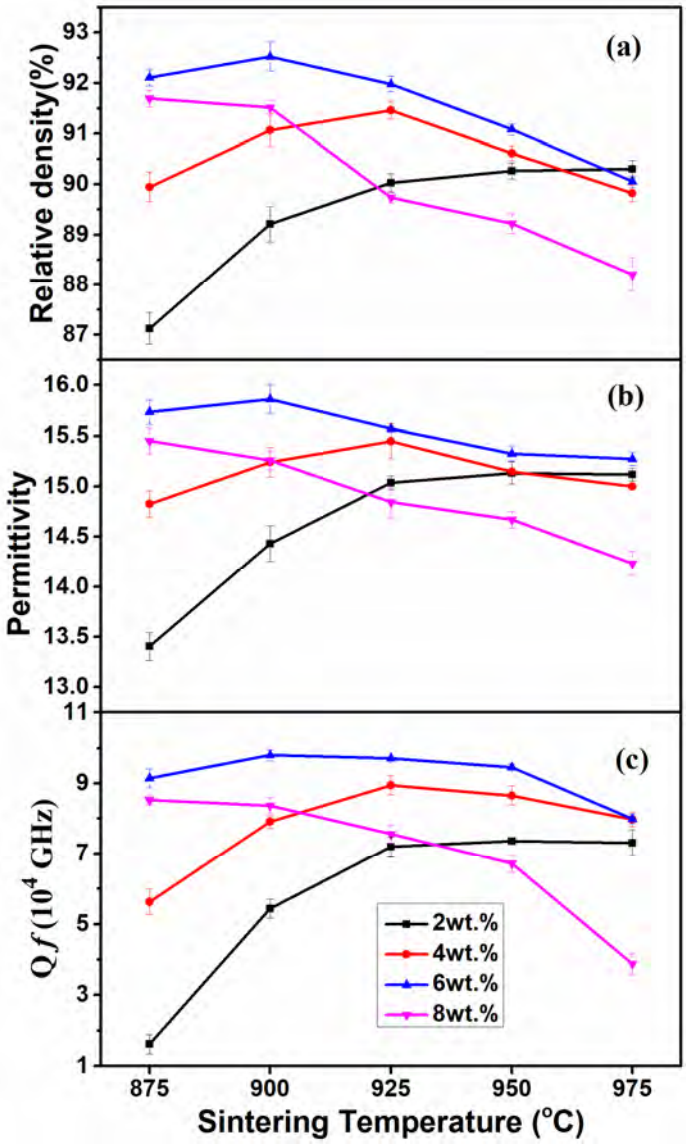
(a)
Relative density(%)
93
92
91
90
89
88
87
(b)
Permittivity
16.0
15.5
15.0
14.5
14.0
13.5
13.0
(c)
Qf (10^4 GHz)
11
9
7
5
3
1
2wt.%
4wt.%
6wt.%
8wt.%
875
900
925
950
975
Sintering Temperature (°C)

Fig. 12

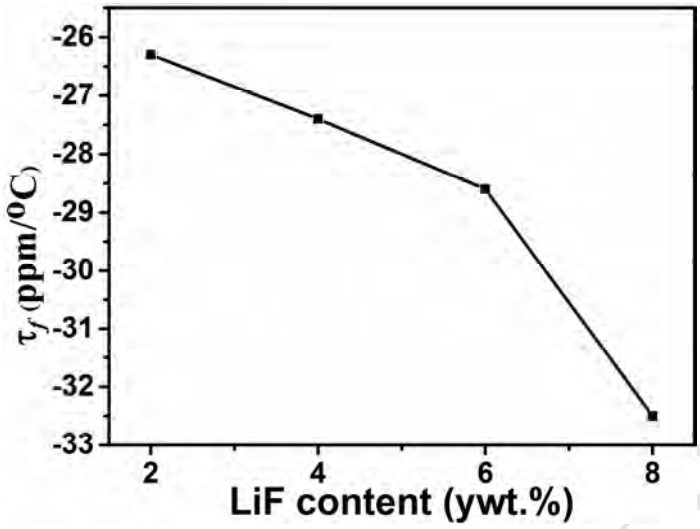

Fig. 13

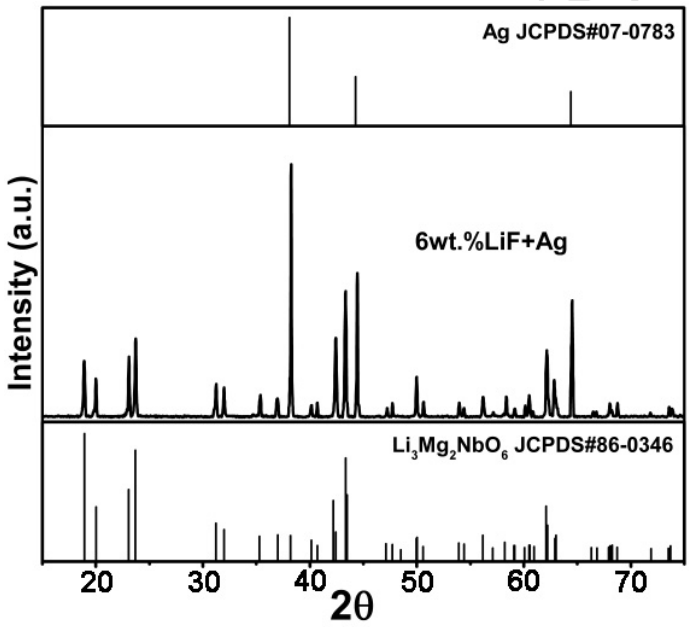

Fig. 14

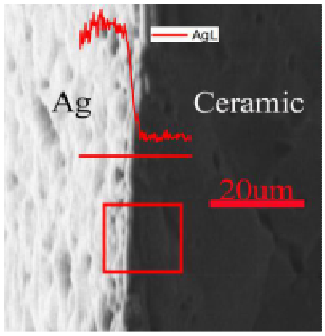

Fig. 15

Microwave dielectric properties of $Li_3(Mg_{1-x}Ca_x)_2NbO_6$ ceramics are investigated.

- ε_r, τ_f correlate with the porosity-corrected permittivity ε_{pc}.
- $Q \times f$ is related to the bulk density, particle size and distribution of grain size.
- Various amounts of LiF additives are used as sintering aid to reduce the sintering temperature.
- The composition could be compatible with Ag electrode.